Please cite this document as:

Slavchov, R.I., Salamanca, M., Russo, D., Salama, I., Mosbach, S., Clarke, S.M., Kraft, M., Lapkin, A.A., Filip, S.V., (2020). The role of NO_2 and NO in the mechanism of hydrocarbon degradation leading to carbonaceous deposits in engines. Fuel *In Press*.

The role of NO_2 and NO in the mechanism of hydrocarbon degradation leading to carbonaceous deposits in engines

Radomir I. Slavchov[1,2*], Maurin Salamanca[2], Danilo Russo[2], Ibrahim Salama[3], Sebastian Mosbach[2], Stuart M. Clarke[3], Markus Kraft[2,4,5], Alexei A. Lapkin[2,5], Sorin V. Filip[6]

[1] *School of Engineering and Materials Science, Queen Mary University of London, Mile End Road, London E1 4NS, UK*
[2]*Department of Chemical Engineering, University of Cambridge, West Site, Philippa Fawcett Drive, Cambridge, CB3 0AS, UK*
[3]*BP Institute, University of Cambridge, Cambridge, CB3 0EZ, UK*
[4] *School of Chemical and Biomedical Engineering, Nanyang Technological University, 62 Nanyang Drive, Singapore 637459*
[5]*CARES – Cambridge Centre for Advanced Research and Education in Singapore, CREATE Tower, 1 CREATE Way, Singapore 138602*
[6] *BP Formulated Products Technology, Research and Innovation, Technology Centre, Pangbourne, UK*

**Corresponding author:* r.slavchov@qmul.ac.uk

Abstract

A hypothetical mechanism of degradation of the fuel droplet leaking out from the injector nozzle in a direct injection combustion engine has been proposed recently. This involves as a key step a radical chain oxidation initiated by NO_2 and branched by nitric oxide, NO, both produced by the combustion. The degradation causes the formation of injector nozzle carbonaceous deposits. The present work gives an experimental validation of some of the assumptions behind this model. An autoclave is used to oxidize isooctane under conditions relevant to the cylinder wall near the nozzle (~150 °C, 10 bar, 5% O_2, 100 molar ppm of NO_2 and 500 molar ppm NO in the gas phase), and the degradation products are monitored via gas chromatography-mass spectrometry (GC-MS). The results show no observable fuel degradation in the absence of NO_x. NO appears to be able to initiate a radical chain by producing NO_2. Nitric oxide also alters the radical chain by transforming the alkyl peroxy radicals (ROO·) to more reactive alkoxy radicals (RO·), resulting in a range of different products. In addition, NO tends to terminate the radical chain by neutralizing a fraction of the alkyl peroxy radicals, producing alkyl nitrates as termination products. The existence of a radical chain is supported by demonstrating the antioxidative action of a radical scavenger. The

chemical reaction mechanism is investigated, based on the detected products, and the key species involved in the degradation process are identified.

Keywords: engine deposits; NO_x; autooxidation; gasoline; radical chain; anti-oxidant

1. Introduction

In a direct injection engine, after the fuel injection, a pool of liquid fuel wets the surface around the nozzle at the cylinder head due to fuel leakage through the seal after the injection [1-4] and residue from the fuel spray. This liquid fuel is exposed to high cylinder pressure (10–30 bar), elevated temperature (100–180 °C at the walls [5]), and to a gas quench layer containing approximately 5-10% oxygen, ~500 ppm (molar) of nitric oxide, NO, and ~100 ppm of NO_2 [4]. Under these conditions, the fuel degrades. Most likely, the initial stages of the injector fouling are dominated by the autooxidation of the fuel film. Later on, soot [3] and up to 10-50% lubricant-derived material [6,7] add to the produced sticky matter, reinforcing the deposit to produce a hard, porous material.

The injector deposits have detrimental effects on the engine operation: they can triple soot emissions in gasoline direct injection engines, and increase NO_x emissions by as much as 40% [8]; the deposits insulate the engine wall causing its temperature to rise [4]; flaked deposits can produce engine "rumble" and knock, and the pores of the deposits can store heavy fuel components, and release them at an inappropriate stage of the engine cycle [9]. The removal of deposits and the prevention of their appearance is a serious issue for the automotive industry. The research into the degradation processes is further stimulated by (i) increasingly stringent emission standards and the resulting stricter requirements for the spray characteristics; (ii) the search for possible renewable biofuel blends for gasoline (e.g., ethyl *tert*-butyl ether [10], and more exotic components [11]), which often result in decreased oxidative stability, potentially leading to accumulation of harmful peroxides; (iii) the detrimental interaction of certain gasoline octane enhancers (such as the toxic N-methyl aniline [12]) with products of gasoline degradation, producing sludge and varnish [12,13].

NO_x produced in the cylinder also cause degradation of the lubricant, and in particular of the gasoline components that accumulate in the lubricant [14-21]. NO_x and gasoline are introduced into the lubricant first at the cylinder walls; further, both NO_x and degraded gasoline pass through the piston rings as blow-by, and cause extensive oxidation of the lubricant in the crankcase, initially producing deposit precursors [20], then resins, sludge and varnish [22]. If either NO_x or gasoline is absent, no varnish is produced [14]. This type of gasoline and NO_x-induced lubricant degradation is responsible for deposition on the piston [14], turbocharger coking [21], and deposits in the lubricant pump.

Decades ago, the typical engine sludge and varnish would have contained significant amounts of N-containing products [14], which was the reason for intensive research on the role of NO_x in the degradation process. A number of *deposit precursors* (primary reaction products of hydrocarbons with NO_x and O_2) that contain nitrogen have been identified [23]: nitro-, nitrate and nitroso functionalities have been reported; some polyfunctional compounds such as 1-nitrate-2-alkanones and alkylhydroxylamines are often mentioned. Later on, in the 1980s, the so-called black sludge became a common problem at the cylinder head [22,24], and it did not appear to be rich in nitrogen. This seems to have resulted in the NO_x degradation mechanism dropping out of fashion. However, the absence of organic N does not mean that NO_x are not involved – notably, if NO_x only initiate and branch the radical chain that oxidizes the gasoline,

then no nitrogen will remain in the degradation products [4]. For example, no organic N-containing compounds were detected in the degraded lubricant in the tests done in Ref. [20], even though NO_x clearly contributed to the degradation.

The details of the fuel degradation process are essential to understand the potential gasoline engine deposit problems, especially with the advance of direct injection spark ignition engines, which can be susceptible to injector nozzle deposits. Various fragmentary hypotheses have been proposed for the degradation mechanism, often questionable and contradictory. Colclough [23] claims that it is NO_2 rather than NO that causes the problem. On the other hand, the lubricant test of Nakamura et al. [25] considered the degradation under the action of NO alone. Moreover, while NO is indeed the weaker initiator, it is more concentrated in the quench layer, and has a branching effect that accelerates the autooxidation [4]. It is unclear to what extent the degradation occurs in the engine cylinder, as opposed to the crankcase and the lubricant lines. There are bench tests for *lubricant* degradation in the presence of NO_2, but these may not be fully representative of the conditions in the quench layer next to the cylinder walls, where the gas phase is a mixture of 5-15% of O_2 with the very potent radical chain initiator NO_2 and the branching agent NO – a test that misses one of these components is likely to produce deposit precursors different from those in the engine. Thus, peroxides and hydroperoxides are considered to be major intermediates of the degradation process [22], but in the presence of NO, the oxidation might proceed through alcohols instead [4]. Both nitrogen oxides react with the reactive intermediates of the radical chain [18]. In Ref. [21], it is assumed that nitrate esters are produced by a reaction of NO_2 with alcohols, and these alcohols are produced from base oil hydrocarbons, but no reaction mechanism has been suggested. Very few tests and models of injector fouling in the literature consider NO_x as a factor driving the *fuel* degradation [4,26]; we are not aware of any experimental data published on NO_x-induced gasoline degradation. It is often the case that the studies on oxidative degradation do not consider specific radical chain initiators at all, e.g., Ref. [27]. Even the most representative tests in the literature that involve all three essential components of the sludge formation, specifically fuel, NO_x and air [18,28,29], might still miss essential physicochemical factors such as the high cylinder pressure that (i) increases the gas phase concentration of NO_x considerably, and (ii) allows the otherwise volatile gasoline components to remain in the liquid state and to undergo nitro-oxidation.

The main aim of this study is to design a bench test to investigate the initial stages of the degradation of gasoline fuel or gasoline components under conditions similar to those occurring at the engine cylinder wall: high pressure, temperature of the order of 150 °C, 5% O_2, with hundreds of ppm of NO_2 and NO each. In accordance with the short review above, several experiments were carried out to assess the role of NO_2, NO and O_2 in the degradation process. The main primary oxidation products (the deposit precursors) are identified. The chemical reactions that lead to these products are analysed.

2. Materials and methods

2.1. Materials

NO and NO_2 balanced with N_2 were supplied by BOC in custom-made 1.5 L cylinders. Three such NO_x-cylinders were used: (i) 1000 ppm NO; (ii) 200 ppm NO_2; and (iii) a mixture of 1000 ppm NO and 200 ppm NO_2. Anhydrous isooctane (99.8%) was purchased from Sigma-Aldrich, and purified by percolation through a packed column containing 100 g of silica gel and 100 g of basic activated alumina under Ar atmosphere. Prior to use, silica gel and alumina were heated for 12 h at 300 °C, as detailed in Ref. [30]. The radical scavenger (2,2,6,6-tetramethylpiperidin-1-yl)oxyl (TEMPO) and the analytical standards for the calibration of acetone and methylpropan-2-ol for gas chromatography-mass spectrometry (GC-MS) were purchased from

Sigma-Aldrich and used as received. The 2,4,4-trimethylpentan-2-ol standard was from TCI, and used as received.

2.2. Reactor

The reaction system has been described previously in Ref. [30], and is shown schematically in Figure 1. Briefly, the 150 mL stainless steel reactor is a batch apparatus with respect to the liquid phase, with continuous bubbling of gas through the liquid. The autoclave was purchased from HEL Ltd. The liquid isooctane (60 mL for each run) was added to a glass insert fitted in the autoclave. The reactor was heated and the temperature was controlled using a hot plate (IKA), with temperature controller (ETS-D5) and aluminium jacket to improve heat transfer. Liquid samples were collected using a stainless steel sampling tube equipped with a ball valve. The outlet of the reactor is connected to a stainless steel condenser kept at -18 °C and 10 bar, to condense the volatile compounds back to the autoclave. Pressure was kept constant using a back pressure regulator (RHPS series dome-loaded regulator by Proportion-Air Inc, with a 0-90 bar calibrated range). For this study, the autoclave was operated at 10 bar and variable temperature, 100-160 °C.

The reactor was equipped with three feeding gas lines (N_2; 10% O_2 in N_2; and a specified concentration of NO_x in N_2) operated through mass flow controllers (SmartTrack 100 Sierra), see Figure 1. Gas flow rates were adjusted to achieve the desired concentrations and the flows were pre-mixed before feeding them to the system through the tubing immersed into the liquid. The gas entering the reactor (a surrogate for the gas in the quench layer next to the engine cylinder wall) contained 95% N_2 and 5% O_2; the concentration of NO was varied between 0 and 500 ppm, and that of NO_2 – between 0 and 100 ppm. For all the experiments, the total gas flow rate was kept at 400 N-mL·min^{-1}, corresponding to 50-60 mL·min^{-1} at 10 bar and 100-160 °C. The head-space volume of the reactor is 90 mL.

A significant fraction of the gas phase in the autoclave is isooctane vapour – using the vapour pressure formula from Ref. [31], the mole fraction of isooctane in the gas phase is obtained as a function of temperature, see Table 1. Thus, 35.3% of the gas phase at 150 °C is isooctane vapour, which has to be accounted for when the gas phase concentrations are calculated – the concentration of component i in the autoclave is computed as $C_i = x_{i0}(1-x_{C8})p/RT$, where x_{i0} is the mole fraction of i in the gas phase before it is introduced in the autoclave, p is pressure, R is the gas constant (cf. supplementary information S1 for a list of symbols). Assuming Henry's constant (liquid concentration/gas concentration ratio) of $K_H^{CC} \approx 1$ for O_2 and NO_x in isooctane, and taking into account the amount of isooctane vapour in the gas phase, we can compute the mean residence time of NO_x and O_2 in the reactor as:

$$\tau = [V^L + (1-x_{C8}) \times V^G] / F, \quad (1)$$

where V^L is the volume of the liquid isooctane (corrected for the thermal expansion), V^G is the volume of the remaining gas, and F is the flow rate in m^3·s^{-1}. This gives τ = 120 s at 160 °C and 170 s at 100 °C (Table 1). The decrease in τ with temperature is due to the increase in the vapour pressure of isooctane. Density of isooctane at each temperature was computed using the empirical formula from Ref. [32], see Table 1.

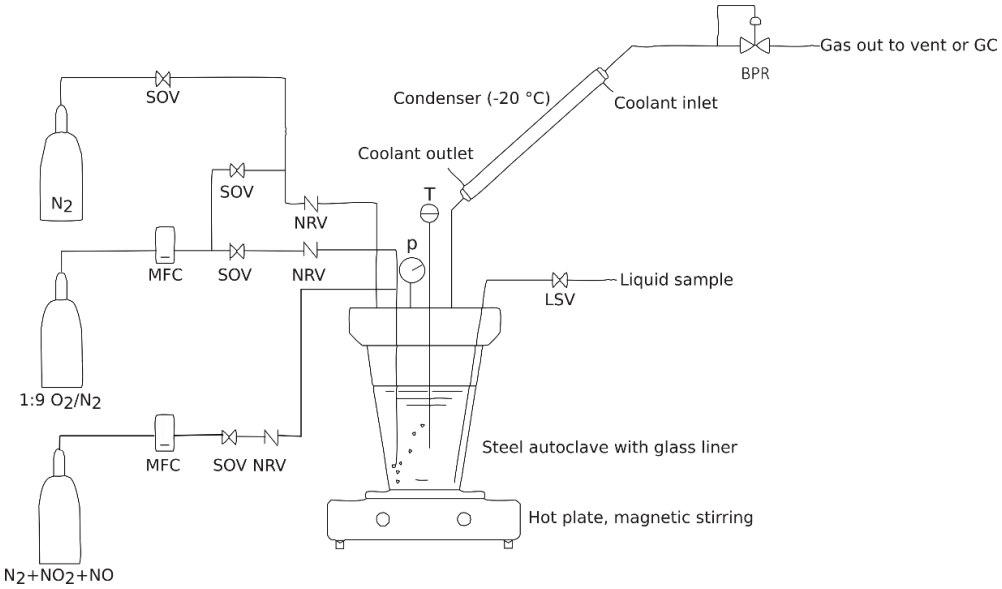

Figure 1. Scheme of the reactor.

Table 1. Conditions inside the reactor.

temperature T [°C]	25	100	120	140	150	160
[a] mole fraction of isooctane in the gas phase, x_{C8}		0.104	0.177	0.284	0.353	0.433
[b] density of liquid isooctane [kg·m^{-3}]	689	622	601	577	564	551
[c] estimated residence time of NO_x, τ [s]		167	152	136	128	120
[d] the CSTR concentration of NO_2 corresponds to feed concentration of NO_2 in ppm of:		294	259	212	183	149

[a] Calculated using the theoretical isooctane vapour pressure formula from Ref. [31]. [b] Calculated using the empirical equation of state of liquid isooctane form Ref. [32]. [c] Computed using Eq (1). [d] Computed via Eq (5).

2.3. Experimental conditions studied

60 mL of isooctane is loaded into the autoclave before sealing. Pure N_2 is fed to the head-space of the reactor until the desired pressure is reached and the initial temperature is established. The gas feed is then switched to a mixture of N_2, O_2, and NO_x through the bubbling line, of composition 5 x% O_2, 95 x% N_2 and specified trace amounts of NO_x. The start of the experiment is the start of the reactive gas flow. The experimental conditions adopted in this investigation, together with the abbreviations for the experimental runs, are summarized in Table 2.

Table 2. A list of conditions and labelling of the experiments.

Test	[NO_2] ppm	[NO] ppm	T °C	[TEMPO] mM
{O_2;T}	-	-	100-160 [a]	-
{O_2;T,Sc}	-	-	100-160 [a]	3.2
{NO_2;T}	100	-	100-160 [a]	-
{NO;T}	-	500	100-160 [a]	-
{NO_2;C}	5-100 [b]	-	150	-
{NO;C}	-	5-500 [b]	150	-
{NO_2+NO}	100	500	150	-
{NO_2+NO;Sc}	100	500	150	3.2

[a] Temperature was increased with time during these experiments, following the profile specified in Figure 4. [b] The concentration of NO_x was increased with time during these experiments, following the profile specified in Figure 5.

The first two tests, {O_2;*T*} and {O_2;*T*,Sc}, were carried out without NO or NO_2. In the second test, {O_2;*T*,Sc}, 3.2 mM (at room temperature) of the radical scavenger, TEMPO, is present in the liquid phase. These experimental runs were devoted to checking the hypothesis that O_2 alone can produce significant oxidative degradation of isooctane under the conditions at the cylinder wall via direct hydrogen atom abstraction, according to the reaction $RH + O_2 \rightarrow R\cdot + HO_2\cdot$. This process has often been assumed to be the key initiation reaction in the autooxidation of fuels, e.g., Ref. [33]. Its rate at 160 °C is 4×10^{-9} M·s^{-1} (corresponding to 8×10^{-9} M·s^{-1} of radicals), according to Arrhenius's parameters from *table 4.1* in Ref. [34] and assuming Henry's constant $K_H^{CC} \approx 1$ for oxygen in isooctane. Such an initiation rate might produce detectable hydrocarbon degradation for lengths of the radical chain in the order of 100 or more. After the start of tests {O_2;*T*} and {O_2;*T*,Sc}, temperature was increased from 100 to 160 °C over 3-3.5 h in a stepwise manner, keeping it at 100, 120, 140, 150 and 160 °C, for ~30 min at each temperature; increasing the temperature from one value to another takes ~10 min (the temperature profile is plotted in Figure 4). Significantly, no products of degradation were detected, both in the presence and in the absence of TEMPO. Note that this is never the case with oxidation of unpurified hydrocarbons: traces of peroxides in them initiate radical chain oxidation of high rate [18].

The next two tests, namely {NO_2;*T*} and {NO_2;*C*}, were performed in order to (i) find conditions at which the reactor could be operated safely but with sufficiently high oxidation rate suitable for further investigation ($|d[O_2]/dt|$ of the order of 10-100 mM·h^{-1}); (ii) identify the products of degradation of isooctane upon initiation by NO_2 but in the absence of NO. The feed concentration of NO_2 in the test {NO_2;*T*} was fixed at 100 ppm, based on the estimation in Ref. [4] for the quench layer concentration at the cold injector wall; temperature was increased stepwise from 100 to 160 °C (as illustrated in Figure 4). The other test, {NO_2;*C*}, was performed at 150 °C (the typical gasoline injector wall temperature), while concentration of NO_2 was increased stepwise from 5 to 100 ppm over ~4 h (the time profile is specified in Figure 5).

Similarly, the tests {NO;*T*} and {NO;*C*} were performed to: (i) investigate to what extent can NO initiate a radical chain alone, without NO_2 in the feed gas, and (ii) find suitable conditions to study the degradation process while the reactor is operated safely. The temperature profile during test {NO;*T*} is the same as for {O_2;*T*} and {NO_2;*T*} above (see Figure 4). The concentration profile during {NO;*C*} corresponds to increasing the concentration from 10 to 500 ppm over ~4 h (Figure 5).

The next test, {NO_2+NO}, corresponds to a feed composition as closely resembling the conditions in the quench layer as possible with our set-up: 100 ppm NO_2 and 500 ppm NO, 150 °C, 10 bar [4]. The last test, {NO_2+NO;Sc}, corresponds to the same conditions but with added radical scavenger, TEMPO, in the liquid phase.

2.4. Detection and calibration

Identification and quantitative analyses of the products in the liquid phase were undertaken on an Agilent 7890GC integrated with a 5977 MSD and fitted with a CTC PAL autosampler. The GC-MS was equipped with a HP-InnoWax column (30 m × 0.250 mm × 0.25 µm). The identity of each compound was established using the NIST MS library and confirmed in some cases by injecting analytical standards. The samples were injected in the GC-MS without further dilution. Inlet temperature was 200 °C. The initial oven temperature was 35 °C, where it was held for 3 min, then ramped at rate 5 K·min^{-1} to 100°C, and subsequently to 200 °C at 20 K·min^{-1}. Split ratio was 50:1 and total analysis time was 21 min. Liquid samples were collected at different experimental times and stored at 4 °C before analysis (performed immediately after the end of each run). The concentrations of acetone, methylpropan-2-ol (C4OH) and 2,4,4-trimethylpentan-2-ol ($C8_4OH$) were followed quantitatively using calibration curves

(concentration vs. integrated signal area; linear regression was used for acetone and quadratic for the alcohols, standard deviation was 0.36 mM for acetone, 1.8 mM for C4OH, 0.28 mM for $C8_4OH$); more details are given in S4. Three isomers of $C8_4OH$ were identified among the products: 2,2,4-trimethylpentan-1-ol ($C8_1OH$), 2,2,4-trimethylpentan-3-ol ($C8_3OH$), and 2,4,4-trimethylpentan-1-ol ($C8_5OH$, cf. Figure 3). We estimated their concentrations by assuming the same signal-to-concentration calibration curve as for the main product, $C8_4OH$. All liquid-phase concentrations reported in this work refer to mM of a species in isooctane at room temperature; the respecive concentrations in the reactor are decreased due to the thermal expansion of the liquid (see Table 1).

2.5. Health and safety measures

The isooctane is flammable and we took measures to work at conditions outside its flammability limits based on data from Refs. [35-40], see the supplementary material S2. In addition, NO_2 and NO are toxic gases; NO_2 and NO sensors were used to detect possible leaks (details are given in supplementary material S3). High concentrations of NO and NO_2 in the presence of water can produce acids (HNO_2, HNO_3) that can damage the GC internals and the column. To avoid this, we conducted the {NO_2;*C*} and {NO;*C*} tests with a slow increase in NO_x concentration, always keeping it at the ppm level, and in the absence of water. We estimated that the maximum concentration of NO_x at which we operate is such that the pH of a water droplet accidentally introduced in the column cannot fall below 3.6 (assuming Henry's constant for NO_x in water of K_H^{CC} ~10).

3. Results

3.1. Level of degradation with and without NO_x

The two tests {O_2;*T*} and {O_2;*T*,Sc}, in which no nitrogen oxides were fed to the reactor, produced no detectable amounts of oxidation products. In all other tests, {NO_2;*T*}, {NO_2;*C*}, {NO;*T*}, {NO;*C*}, {NO_2+NO}, and {NO_2+NO;Sc}, significant degradation of the isooctane was evident, and more than 70 separate chromatographic peaks have been detected. The concentrations of the three components we followed reached up to 25 mM for 2,4,4-trimethylpentan-2-ol, 16 mM for acetone, and 16 mM for methylpropan-2-ol (Figure 4). The levels of degradation after the end of these six tests are of the same order of magnitude, and similar GC peaks appear, see the sample chromatogram comparison in Figure 2. There are, however, many important exceptions that are discussed below.

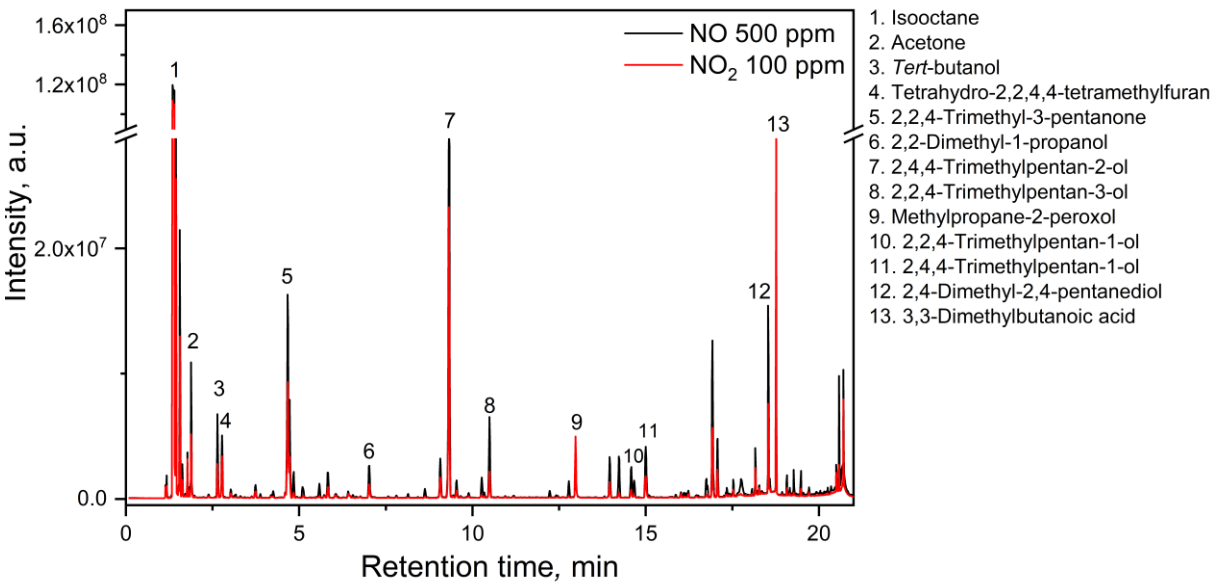

Figure 2. Chromatogram for nitro-oxidation of isooctane with 500 ppm NO or 100 ppm NO_2. Probes from tests {NO;*T*} and {NO_2;*T*}, respectively, taken 163 min after the start of the tests (33 min after 150 °C has been reached, cf. Figure 4).

3.2. Reaction chemistry

To interpret our results for the composition of the nitro-oxidized isooctane, we formulated a reaction mechanism of the process, based on the theory of low-temperature radical chain autooxidation [34,38]. The mechanism produces a set of key reactive intermediates which could be inferred from the structure of the identified products. For the sake of brevity, we present the mechanism first, and below our evidence is provided. A simplified reaction scheme of oxidation of isooctane is shown in Figure 3. *The first step* is the abstraction of hydrogen (aH) from isooctane by either RO_2·, RO·, or NO_2. It produces four isomers of isooctyl (2,2,4-trimethyl-x-pentyl), corresponding to the four distinct carbon atoms from which a H-atom can be abstracted (C_1, C_3, C_4 or C_5). Abstraction by the alkyl peroxy radical RO_2· is highly selective and is expected to produce mostly *tert*- and some *sec*-isooctyl (2,2,4-trimethyl-4-pentyl and 2,2,4-trimethyl-3-pentyl). In contrast, the more reactive alkoxy radical RO· should produce all four isooctyl isomers in similar quantities [38]. Thus, if aH is dominated by RO_2·, the aH-C_4-route in Figure 3 will be significantly faster than the other three routes; if aH is dominated by RO·, the radical chain will produce the products of all four degradation routes.

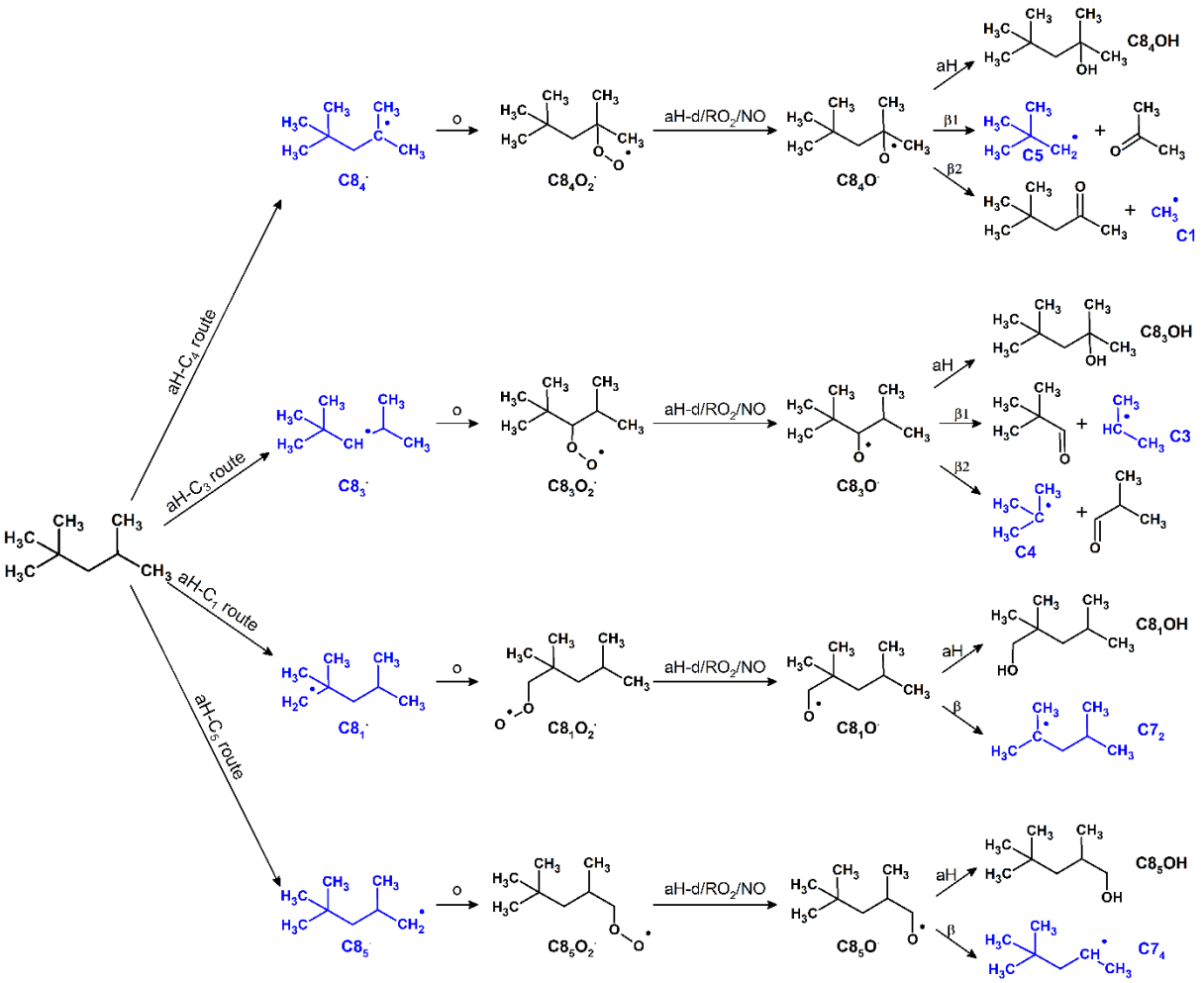

Figure 3. Reaction mechanism of isooctane and oxygen – main reactions. The key alkyl radicals formed are in blue.

The main *second step* is the oxidation (o) of the alkyls. It produces four alkyl peroxy radicals (isooctyl + O_2 → isooctylO_2·). These radicals are relatively long-lived and participate in a number of reactions: terminations with other radicals, inter- and intramolecular hydrogen abstraction, and other rearrangements [34,38]. However, it seems that under the conditions at the wall of the cylinder, the main *third step* is the transformation of the alkyl peroxy radical to alkoxy radical via one of three possible routes [4,18,34,38,41]:

(i) reaction with NO: $RO_2\cdot + \cdot NO \rightarrow ROONO \rightarrow RO\cdot + \cdot NO_2$;

(ii) aH and decomposition: $RO_2\cdot \rightarrow RO_2H \rightarrow RO\cdot + HO\cdot$;

(iii) reaction with RO_2·: $2RO_2\cdot \rightarrow RO_4R \rightarrow 2RO\cdot + O_2$. (2)

Given the high rate of the first reaction, we previously hypothesized that, in the presence of NO, the rate-determining aH step of the radical chain will be dominated by RO· (so that aH is RO· + RH → ROH + R·). This is in contrast to the common RO_2·-dominated radical chains (where aH is $RO_2\cdot$ + RH → RO_2H + R·) that has been widely studied in the literature [33,34,38]. In the *fourth step*, the isooctoxy radicals (RO·) either abstract hydrogen atom from isooctane to produce the respective alcohols (which are the main primary products of oxidation), or break into an alkyl radical and an aldehyde/ketone via a β-scission reaction.

According to the mechanism in Figure 3, a pool of 10 key alkyl radicals is present in the mixture:

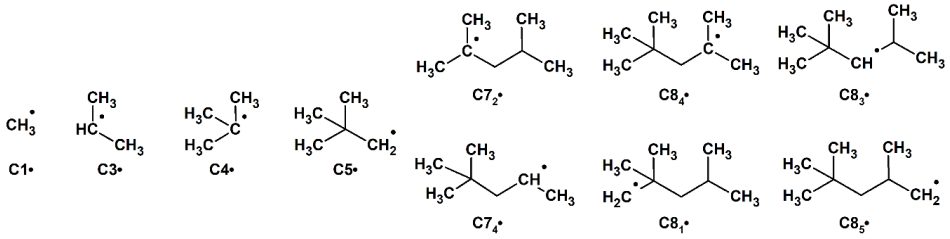

(3)

We use the following notation to denote these species: C1 (methyl), C3 (2-propyl), C4 (methyl-2-propyl), C5 (dimethyl-1-propyl), $C7_2$ (2,4-dimethyl-2-pentyl), $C7_4$ (4,4-dimethyl-2-pentyl), $C8_x$ (2,2,4-trimethyl-x-pentyl, where x = 1,3,4,5). All products that we were able to identify via GC-MS can be traced back to these radicals, or to their alkyl peroxy (RO_2·) or alkoxy (RO·) derivatives.

In the following, the main reactions and products are discussed.

3.3. Initiation

The ability of NO_2 to abstract hydrogen from alkanes and initiate a radical chain oxidation is well-known, e.g., *sec. 3.3.2* of Ref. [34] and Ref. [18]. Contrarily, NO is not known as a potent initiator. It is, therefore, not immediately clear what initiated the radical chain (i.e. abstracted hydrogen from isooctane) in tests {NO;*T*} and {NO;*C*}, where no NO_2 was fed to the autoclave. Time dependences of the experimentally determined concentration of 2,4,4-trimethylpentan-2-ol in tests {NO_2;*T*} and {NO;*T*} are compared in Figure 4a (note that this concentration probably includes a fraction of the unstable 2,4,4-trimethyl-2-hydroperoxypentane which might produce the alcohol in the GC column). As evident, the concentration profiles are similar. Since NO_2 is at 100 ppm, while NO is at 500 ppm, we can conclude that NO_2 produced 5-fold higher degradation rate than NO in these tests. Likewise, in the tests {NO;*C*} and {NO_2;*C*}, the first quantifiable amounts of acetone and 2,4,4-trimethylpentan-2-ol appeared at 20 ppm of NO_2, while 5-fold higher concentration of NO (100 ppm) is required for degradation products to be detected in {NO;*C*} (Figure 5 and Figure 6). The temperature in the tests {NO_2;*T*} and {NO;*T*} increases from 100 to 160 °C, yet concentration of 2,4,4-trimethylpentan-2-ol in Figure 4a follows a similar trend, which suggests also a similar temperature dependence of the rate of production of this alcohol for the NO- and the NO_2-initiated processes.

These results can be explained with the oxidation of NO inside the autoclave in the reaction

$$2NO + O_2 \rightarrow 2NO_2. \quad (4)$$

This process produces enough NO_2 to explain the observed degradation. The reaction follows the apparent rate law $r = k[NO]^2[O_2]$; the rate decreases with the rise in temperature, due to the slightly negative temperature dependence of k [42]. To estimate the resulting concentration of NO_2 in the reactor, we assume that the reaction (4) proceeds as if the involved reactants are in an ideal continuous-stirred tank reactor (CSTR). Under this assumption, and neglecting the nitrogen oxides consumed by the autooxidation of isooctane, the mass balance of NO reads [43]:

$$\frac{[NO]_0 - [NO]}{\tau} = 2k[NO]^2[O_2]. \quad (5)$$

Here $[NO]_0$ is the initial concentration in the autoclave, after dilution with isooctane vapours, and τ is the mean residence time of NO in the reactor (Table 1). Henry's constant of both O_2 and NO are assumed $K_H^{CC} \approx 1$. The quadratic equation (5) determines [NO]. The respective produced amount of nitrogen dioxide is found from the mass balance $[NO_2] = [NO]_0 - [NO]$. Using the rate constant from Ref. [42], $k\,[M^{-2}s^{-1}] = 1200\times\exp(530/T[K])$, we find $[NO_2]$ that corresponds to a feed concentration 149 ppm at 150 °C and 500 ppm NO (after correcting for the isooctane vapours). Similar estimates are given in Table 1 for other temperatures, and in

Figure 5 for different $[NO]_0$. These numbers are an upper limit estimate for $[NO_2]$: in the real reactor, the concentration of NO_2 in the bubbles right at the exit of the bubbling line will be almost zero while the one in the gas phase above the liquid isooctane should be closer to the CSTR value. The saturation of the liquid phase is likely to correspond to a NO_2 level in the middle between these two limits, i.e. roughly half the CSTR value. Thus, the quantity of NO_2 in tests {NO;*T*} and {NO_2;*T*} is of the same order of magnitude. The tests provided no evidence of direct hydrogen abstraction by NO (RH + NO → R· + HNO). For example, in {NO_2;*C*}, the 2,4,4-trimethyl-2-pentanol reaches concentrations above 1 mM only after the feed NO_2 level reached 50 ppm; in {NO;*C*}, the same product exceeded 1 mM after the feed NO level reached 200 ppm, corresponding to 44 ppm NO_2, calculated through Eq (5), see Figure 5 and Figure 6. This would not be the case if NO contributed significantly to the initiation.

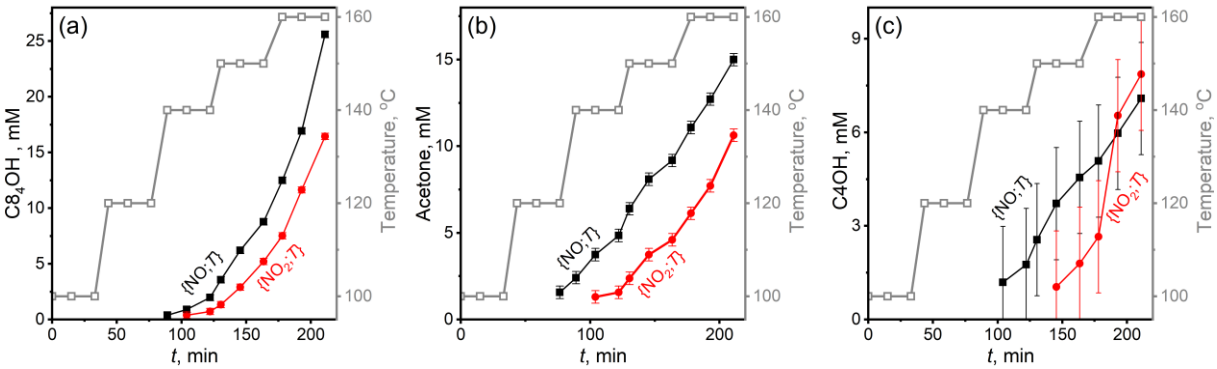

Figure 4. Time evolution of the concentrations in the liquid isooctane of (a) 2,4,4-trimethylpentan-2-ol, $C8_4OH$; (b) acetone; and (c) methylpropan-2-ol, C4OH. Comparison between tests {NO;*T*} (black squares) and {NO_2;*T*} (red circles). Temperature increases with time from 100 to 160 °C, following the same profile (open squares, right axis). Gas feed concentrations: $[NO]_0$ = 500 ppm, $[NO_2]_0$ = 100 ppm.

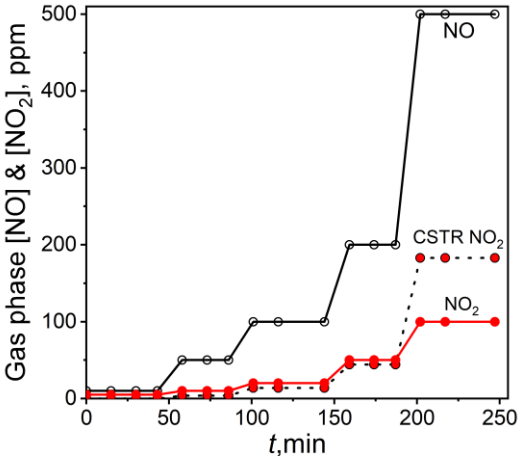

Figure 5. Concentration profiles in tests {NO_2;*C*} (red line) and {NO;*C*} (black lines). The points indicate where samples have been taken from the liquid phase for analysis. The plateau values for NO_2 correspond to 5, 10, 20, 50 and 100 ppm; for NO, these are 10, 50, 100, 200, 500 ppm. The dashed line "CSTR NO_2" is the estimated level of NO_2 in test {NO;*T*}, due to the oxidation reaction $2NO + O_2 \rightarrow 2NO_2$, see Eq (5).

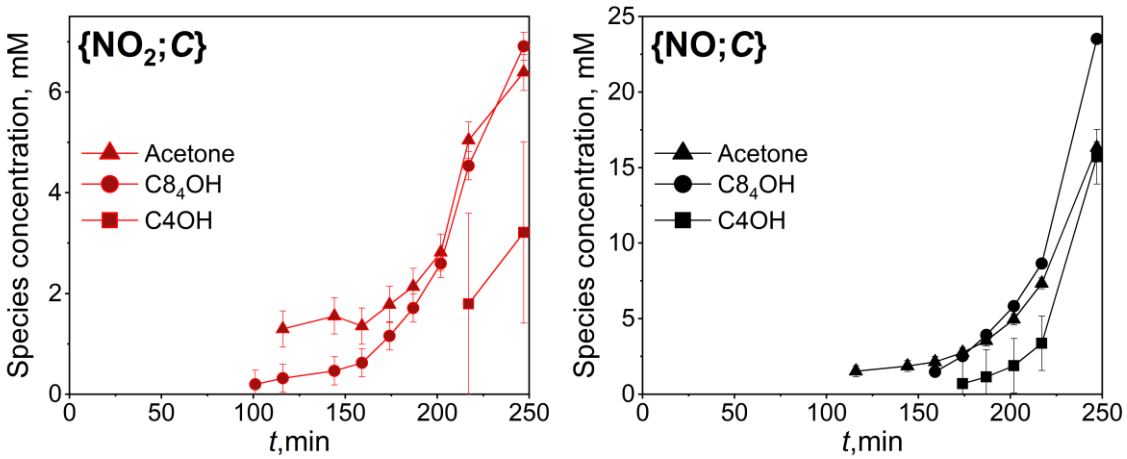

Figure 6. Evolution of the concentrations of 2,4,4-trimethylpentan-2-ol ($C8_4OH$), acetone, and methylpropan-2-ol (C4OH) in tests {NO_2;*C*} and {NO;*C*}.

3.4. Hydroperoxides

The alkyl radicals (3) react with oxygen to produce the corresponding alkyl peroxy radicals RO_2·, which can abstract hydrogen from isooctane to produce ten respective hydroperoxides RO_2H. Most of these are unstable under the conditions of the experiments and decompose via the reaction (2)-(ii). The three tertiary hydroperoxides are an exception: methylpropane-2-peroxol ($C4O_2H$); 2,4-dimethylpentane-2-peroxol ($C7_2O_2H$), and 2,4,4-trimethylpentane-2-peroxol ($C8_4O_2H$). $C4O_2H$ was detected in significant quantities in all experiments (e.g., peak #9 in Figure 2); the chromatographic peaks of $C7_2O_2H$ and $C8_4O_2H$ could not be identified.

3.5. Alcohols

The reactions (2) transform the alkyl peroxy radicals, RO_2·, to ten alkoxy radicals, RO·, that readily abstract hydrogen from isooctane to form the respective ten alcohols. All alcohols but the two most volatile have been detected: we could not identify peaks corresponding to methanol or 2-propanol in the liquid phase.

The primary isooctanols $C8_1OH$ and $C8_5OH$ are abundant in all runs in which NO was present in the gas phase. In comparison, their concentration was lower in tests {NO_2;*T*} and {NO_2;*C*}. Similarly, the secondary isooctanol $C8_3OH$ is of lower quantity in {NO_2;*T*} than in {NO;*T*}; at the same time, the amount of $C8_4OH$ is similar, Figure 4a. To give an estimate of the amounts of $C8_xOH$, we assumed that the relationship signal-to-concentration from the calibration curve of $C8_4OH$ is roughly applicable to the other three alcohols. This is probably not true – to begin with, the isomers have vastly different retention times ($\tau_{retention}$ = 9.3, 10.5, 14.6, 15.0 min for $C8_4OH$, $C8_3OH$, $C8_1OH$ and $C8_5OH$, respectively). Nevertheless, this approach allows us to make a comparison between the different tests. The concentrations obtained from the assumed calibration curves are plotted in Figure 12 in S4. At the end of test {NO;*T*}, the ratio of the three alcohols corresponds to selectivity ratios of $[C8_4OH]:[C8_3OH]/2 = 16$ and $[C8_4OH]:([C8_1OH] + [C8_5OH])/15 = 89$ (i.e. hydrogen atoms are abstracted 16 times faster from tertiary carbon than from secondary, and 89 times faster than primary; 2 and 15 are the number of secondary and primary C–H bonds in isooctane). In comparison, in test {NO_2;*T*}, these are $[C8_4OH]:[C8_3OH]/2 = 34$ and $[C8_4OH]:([C8_1OH] + [C8_5OH])/15 = 153$, i.e. oxidation in the absence of NO is about twice as selective.

The selective production of the tertiary alcohol in the absence of NO is explained with reaction (2)-(i): the nitric oxide produces RO· from RO_2·. Consequently, when NO is present, the hydrogen abstraction step of the radical chain will transfer H from isooctane to the reactive

non-selective RO·, while in the absence of NO, the hydrogen abstraction will proceed mostly through RO_2· and tertiary C–H bond [38].

3.6. Aldehydes and acids

Aldehydes can be produced either directly from oxidation of the primary key radicals C1, C5, $C8_1$, and $C8_5$ (e.g., $RCH_2· + O_2 \rightarrow RCH_2O_2· \rightarrow RCH·O_2H \rightarrow RCHO + HO·$ [44]), or by β-scission of the alkoxy radicals C3, C5, $C7_4$, $C8_1$, $C8_3$, and $C8_5$ (as in the fourth step in Figure 3). Let us use for the first process the term C_1o-route, and for the second – the β-route. Most of the possible aldehyde products can be formed via one route only; formaldehyde and dimethylpropanal can be formed via both:

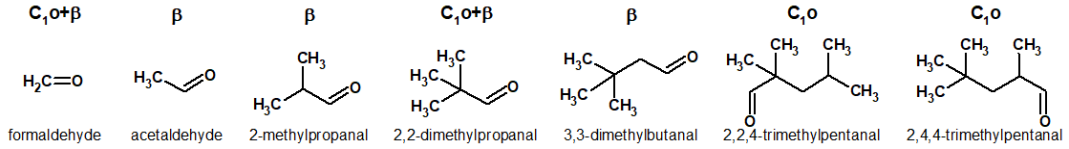

(6)

Dimethylpropanal is the only aldehyde we detected in the liquid phase. The probable reason for the absence of aldehydes is that they are easily oxidized to the respective acids [34,38]. Three of these acids were identified: methylpropionic, dimethylpropionic and 3,3-dimethylbutanoic, corresponding to the 3rd, the 4th and the 5th aldehyde in the list (6). Two major late peaks in the chromatograms might well be the two isooctanoic acids, but we could not ascertain that. Formic acid was not detected, but we identified small quantities of some esters of it with the alkanols present: C4OCOH, C5OCOH and $C8_5$OCOH.

The evolution of the concentration of the acids is somewhat similar to that of methylpropan-2-ol in Figure 4(c). Without NO (tests {NO_2;*T*} and {NO_2;*C*}), the acids appear at an earlier stage compared to {NO;*T*} and {NO;*C*}. This can be explained with lower rate of route C_1o in the absence of NO: this route requires primary radicals, which are of low concentration in RO_2·-dominated radical chain, see section 3.5. The rate of the β-route is also higher in the presence of NO, as it starts with β-scission of RO· produced in reaction (2)-(i) from NO. Although they appear later, the final concentrations of acids are significantly higher in the absence of NO than in its presence (as illustrated by the selectivity ratios computed in Table 3 in S4). A tentative explanation is that NO produces more acidic medium and catalyses secondary reactions depleting the acids, e.g., esterification.

3.7. Ketones

Ketones can be produced either by direct oxidation of the primary key radicals C3, $C7_4$, and $C8_3$ (e.g., via $R_1R_2CH· + O_2 \rightarrow R_1R_2CHO_2· \rightarrow R_1R_2C·O_2H \rightarrow R_1R_2CO + HO·$ [44], C_2o-route) or by β-scission of the alkoxy radicals C4O·, $C7_2$O·, and $C8_4$O· (as in Figure 3; β-route). A third possibility, the R_3O_2-route, is ketone production through intramolecular rearrangement with alkyl transfer of the peroxide radicals $C4O_2$·, $C7_2O_2$·, and $C8_4O_2$· [44] and subsequent scission, via the reactions $R_1R_2R_3CO_2· \rightarrow R_2R_3C·O_2R_1 \rightarrow R_2R_3C{=}O + ·OR_1$. Four ketone products are possible in theory:

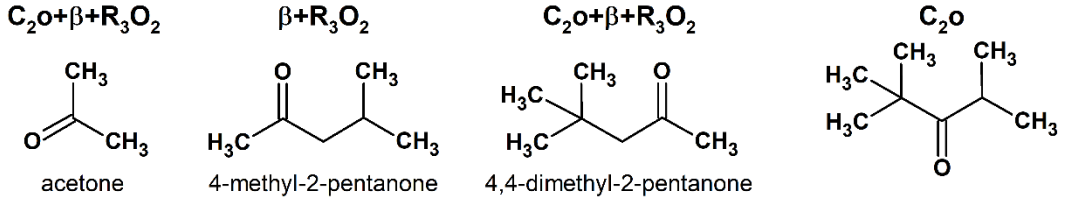

(7)

All but the second product (4-methyl-2-pentanone) were identified, and are present in all experiments.

Acetone is one of the main products of the oxidation: in Figure 6a, it is seen that in test {NO_2;*C*} acetone is more concentrated even than $C8_4OH$. The evolution of its concentration is illustrated in Figure 4b, for tests {NO_2;*T*} and {NO;*T*}. Based on these data, it can be concluded that acetone forms at higher *T* when NO_2 instead of NO is fed to the reactor, suggesting that the β-scission process that produces acetone (Figure 3) has a lower rate without NO. This is explained with the lower concentration of RO· radicals when NO is present, due to the process $RO_2\cdot + NO \rightarrow RO\cdot + NO_2$.

3.8. Radical isomerization

Both peroxide and alkoxy radicals can undergo intramolecular radical abstraction reactions [34,38], producing 24 hydroperoxyalkyl (listed in Figure 11 in S4) and 24 respective hydroxyalkyl radicals from the key alkyls (3). These 48 radicals produce a large number of polyfunctional compounds, most of which are hard to separate and identify. Only the following could be identified.

a) Diols and hydroxyalkanones. Two diols were detected. A detectable quantity of 2,2,4-trimethylpentan-1,3-diol was produced in tests {NO;*T*}, {NO_2+NO}, and {NO_2+NO; *T*}. Its appearance is straightforward to explain (Figure 7b): a hydroperoxyalkyl or hydroxyalkyl is oxidized to alkyl dihydroperoxides, hydroperoxy alcohols and diols, following a process similar to those in Figure 3. The hydroperoxy groups then degrade to hydroxyl via Eq (2)-(ii). A much larger peak, however, corresponds to a product identified as 2,4-dimethylpentane-2,4-diol; for its production, there are at least 3 possible routes, shown in Figure 7a. It is likely that the process includes a step $RCH_2O\cdot \rightarrow R\cdot$, either by β-scission or via more complicated mechanism. Both diols are of lower quantity in the absence of NO (see Table 3 in S4). This is due to the lower rate of formation of primary alkyl and hydroperoxyalkyl radicals in the absence of NO.

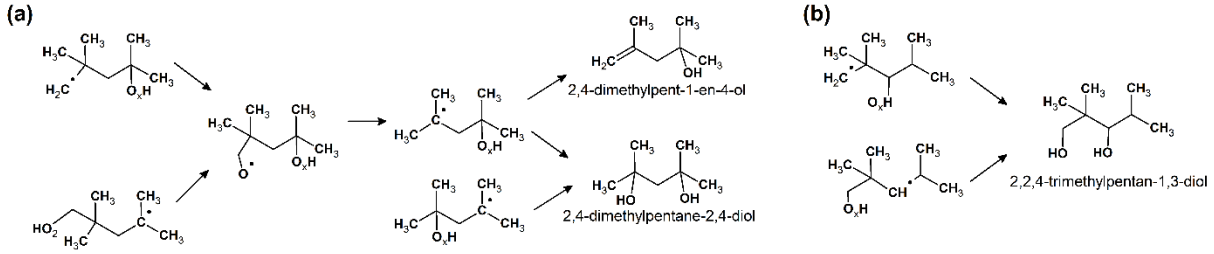

Figure 7. Mechanism of formation of the identified (a) diols, and (b) enol from the key hydroperoxyalkyls and hydroxyalkyls (cf. Figure 11 in S4). $–O_xH$ can be either –OH or $–O_2H$.

In addition, two hydroxyalkanones were detected: 4-methyl-4-hydroxypentan-2-one, which has a significant peak in the chromatogram, and traces of 2,4-dimethyl-2-hydroxypentan-3-one. Both compounds can be obtained via a latge number of routes that resemble those in Figure 7. It might be that 4-methyl-4-hydroxypentan-2-one is a product of dimerization of acetone [45,46].

b) Alkenes. The β-hydroperoxyalkyl radicals decompose according to the reaction [44]:

$$>C\cdot–C(O_2H)< \rightarrow >C=C< + HO_2\cdot. \quad (8)$$

Eight different alkenes can be produced in this way: propene (from C3), methylpropene (from C4), several isomers of heptene, 2,4,4-trimethyl-1-pentene (from $C8_4$ and $C8_5$), and 2,4,4-trimethyl-2-pentene (from $C8_3$ and $C8_4$). Three of these products were detected – the methylpropene and the 2,4,4-trimethyl-x-pentenes. The alkenes are found in larger quantities in the absence of NO (cf. Table 3 in S4). The reason is again the RO·-dominated chain in {NO;*T*} and {NO;*C*}: the reaction (8) is starting from peroxide radicals, therefore, its rate decreases when NO is present. The alkenol 2,4-dimethylpent-1-en-4-ol has also been detected; it is likely the product of the same type of reaction, see Figure 7a.

c) Heterocyclic products. The hydroperoxyalkyls are known to take part in cyclization reaction to form cyclic ethers with release of HO· [44]. Three products of this type have been identified:

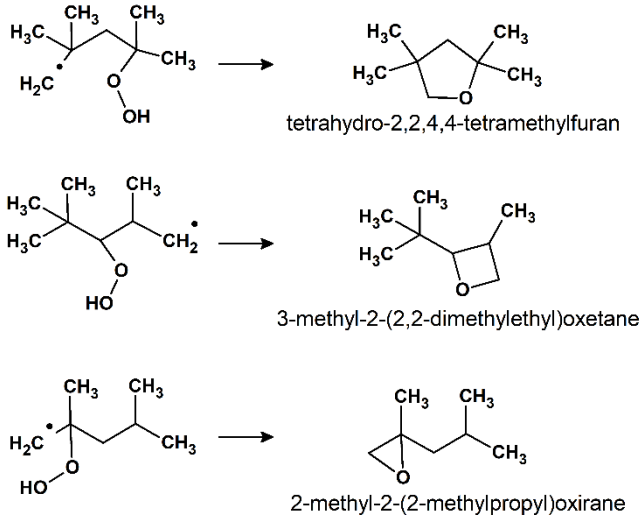

(9)

The tetrahydro-2,2,4,4-tetramethylfuran seems to be an important product, see Figure 2. This ether is detected at an earlier time and is of higher concentration in the absence of NO, which is explained with the need for a hydroperoxy group for the cyclization to take place. On the contrary, 3-methyl-2-(2,2-dimethylethyl)oxetane is more concentrated in {NO;*T*} than in {NO_2;*T*}. The probable reason is that 2,2,4-trimethyl-3-hydroperoxy-5-pentyl is formed from the secondary 2,2,4-trimethyl-3-pentyl: the latter is expected to be more concentrated in {NO;*T*} than in {NO_2;*T*}, due to the selectivity of the hydrogen abstraction in {NO_2;*T*}. In addition, small quantities of 2-methyl-2-(2-methylpropyl)oxirane were detected in {NO;*T*}.

d) Other products and reaction routes. Small amounts of 4-methylpent-3-en-2-one were detected in test {NO_2+NO}, most probably as a result of the reaction (*p. 258* of [44]):

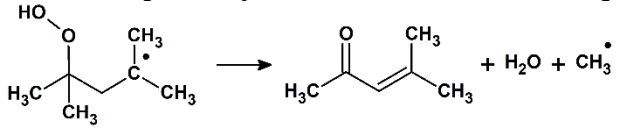

(10)

We detected traces of another conjugated carbonylalkene, (2,2-dimethyl)propylpropenal, in some of the experiments.

3.9. Nitrate esters and nitroalkanes

A striking difference between nitro-oxidation with and without NO is that when the nitric oxide is present, it produces many organic N-containing compounds, while NO_2 alone does not, under the conditions of our experiments. Significant amounts of alkyl nitrates were detected, including the methylethyl and the 3,3-dimethylpropyl esters of nitric acid ($C3ONO_2$ and $C5ONO_2$). None of these were detected in the absence of NO. The nitrates are probably produced by isomerization of alkylperoxynitrite [18,41], via the scheme:

$$RO_2\cdot + \cdot NO \rightarrow ROONO \rightarrow RONO_2. \quad (11)$$

The formation of $RONO_2$ is very likely to be important for the rate of the oxidation process, as it is a termination reaction, i.e. nitric oxide has an anti-oxidant radical scavenging effect. This is compensated to a large extent by the competing process $RO_2\cdot + \cdot NO \rightarrow ROONO \rightarrow RO\cdot + \cdot NO_2$, reaction (2)-(i), which produces reactive RO· that accelerate the hydrogen abstraction and, consequently, the rate of autooxidation [4].

In addition to nitrates, several nitro compounds have been identified: the 2,2,4-trimethyl-4-nitropentane ($C8_4NO_2$) was in quantifiable amount whenever NO was present in the reactor, but was absent in tests {NO_2;*T*} and {NO_2;*C*}; traces of nitromethane and 2-methyl-2-

nitropropane ($C1NO_2$ and $C4NO_2$) were also detected in {NO;*T*}. One bifunctional product, 1-nitromethylpropan-2-ol, has been detected, again only if NO is present in the reactor. The mechanism producing these nitroalkanes and nitroalkanol is unclear.

Our finding that no N-containing products are formed in the absence of NO can be compared with the results of Johnson and Korcek [18], who passed gas containing 20% O_2, 180 ppm NO_2, and 10 ppm NO through hexadecane at 160 °C, 1 atm. These authors found that most of the NO_x entering their reactor appear to remain bound in nitro-oxidation products; this is hardly in agreement with our results, in view of the low level of NO in their experiments. A possible reason for the difference is the high amount of peroxides present initially in their hexadecane – the radical chain in their experiments is driven mainly by these peroxides (see *fig. 1* in Ref. [18]). Indeed, when oxidation products are already present in the isooctane, NO_2 is preferentially consumed by binding to oxidation intermediates [18]; otherwise it abstracts hydrogen from hexadecane.

3.10. Effect of the antioxidant

3.2 mM of the radical scavenger TEMPO added to the isooctane results in approximately 2.5 times smaller amount of oxidation products in test {NO_2+NO;Sc} compared to {NO_2+NO}, Figure 8. This means that the length of the radical chain in {NO_2+NO} is at least 3.5, i.e. every initiation event RH + $\cdot NO_2 \rightarrow R\cdot + HNO_2$ results in the production of at least 3.5 oxidized hydrocarbon molecules. The antioxidant also influences the selectivity of the reactions – the TEMPO-produced change of selectivities relative to $C8_4OH$ are given in Table 3 in S4 for a list of products. According to the values of these selectivities, the first noticeable effect is that the formation of acetone and especially *tert*-butanol is decelerated to a greater extent than the formation of the main product, $C8_4OH$. *More* alkenes are produced when the antioxidant is present. Also, the amount of nitrates and nitrocompounds decreases only moderately or remains similar in the presence of the scavenger.

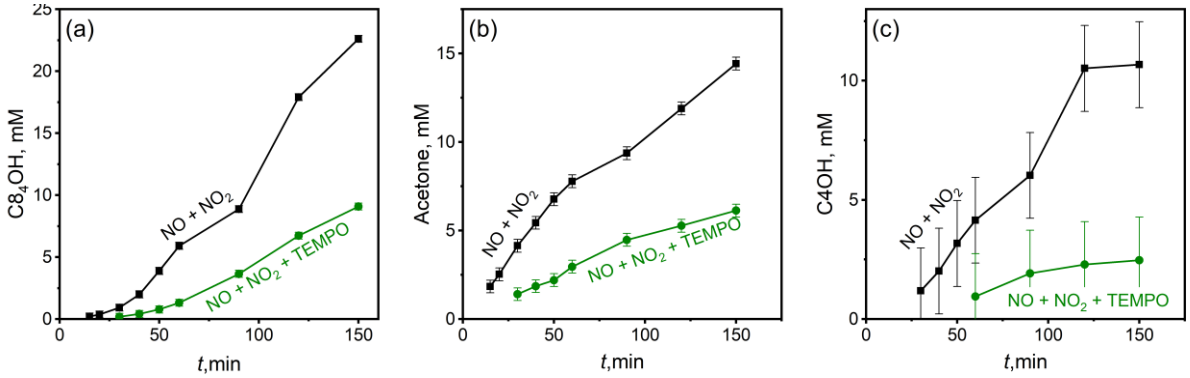

Figure 8. Effect of 3.2 mM of radical scavenger TEMPO in the liquid isooctane on the evolution of the concentrations of (a) 2,4,4-trimethylpentan-2-ol; (b) acetone, and (c) methylpropan-2-ol. T = 150 °C, p = 10 bar, feed concentrations [NO_2] = 100 ppm, [NO] = 500 ppm, [O_2] = 5 x%; tests {NO_2+NO} (black squares) and {NO_2+NO;Sc} (green circles).

TEMPO slowly disappears in the presence of NO_x. Several chromatographic peaks can be related to degradation products stemming from TEMPO, but none of these compounds could be identified with certainty. We evaluated the concentration of TEMPO as a function of time in Figure 9 (assuming linear dependence of TEMPO's peak area on its concentration). The dependence [TEMPO] vs. t is linear; the slope in Figure 9 corresponds to rate constant k = 0.0185±0.0013 mM/min. The data suggest zeroth order kinetics, but this conclusion requires additional verification. For the time of the experiment, 2.6 mM of TEMPO is depleted.

This is by an order of magnitude smaller than the decrease of the concentration of oxidation products in Figure 8. This suggests, together with the estimate of the radical chain length, that TEMPO is being regenerated after most events of active radical neutralization.

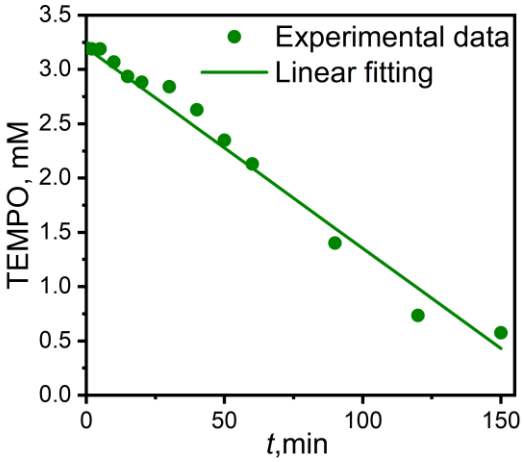

Figure 9. Evolution of the concentration of TEMPO with the advance of test {NO_2+NO;Sc}.

Our results agree with the known mechanism of antioxidant action of TEMPO reported in the literature [47]:

$$>NO\cdot + R\cdot \rightarrow >NOR;$$
$$RO_2\cdot + >NOCR'_2CHR'_2 \rightarrow RO_2H + >NO\cdot + CR'_2{=}CR'_2, \qquad (12)$$

Here, >NO· is the active aminoxyl group of TEMPO. In the first step, it binds to any alkyl present in the mixture, see scheme (3). If the alkyl has a CH bond in α-position, then >NOR can further react with RO_2· to produce an alkene $CR'_2{=}CR'_2$ and a hydroperoxide RO_2H, and regenerate the antioxidant. This explains the observed increase in concentration of alkenes when TEMPO is present. The second reaction (12) is impossible if R· is C1·, C5·, or $C8_1$·; in addition, TEMPO can degrade by reacting with some of the products of oxidation present [47]. These are possible reasons for the observed depletion in Figure 9. We found no evidence of TEMPO reacting with NO_x; in contrast, significant depletion of phenolic radical-trapping antioxidant have been reported (2,6-di-*tert*butyl-4-methylphenol [18], 2,4,6-tri-tert-butylphenol [48]), by direct reactions with NO_2.

3.11. Reaction rates

This work was not designed as a kinetic study, so we leave the extraction of accurate rate law parameters for the future. Yet, several important conclusions can be made based on the results.

As noted earlier [4], the rate of initiation due to the 5% O_2 present in the quench layer is negligible compared to the rate of initiation due to the reactive NO_2. However, the rate of the process *tert*-RH + NO_2 → *tert*-R· + HNO_2 predicted theoretically based on the parameters in *table 3.10* of Ref. [34] (which we used previously in Ref. [4]) seems to be impossibly high. For example, in test {NO_2+NO}, where 100-280 ppm of NO_2 are present, the theoretical initiation rate is $r_i = k[NO_2][\text{isooctane}] \approx 0.4\text{-}1.4$ mM·s^{-1} (using $k = 4.8$ M^{-1}s^{-1} based on Ref. [34]). The total rate of formation of 2,4,4-trimethylpentan-2-ol and acetone is 0.004 mM·s^{-1}, Figure 8; even if these main two products are only 10% of the total amount, this is still 0.04 mM·s^{-1} of oxidation products. Further, the radical chain length is at least 3.5, so a rough upper-limit estimate of the initiation rate would be 0.01 mM·s^{-1}, which is two orders of magnitude lower than the one predicted theoretically (i.e. the rate constant of *tert*-RH + NO_2 → *tert*-R· + HNO_2 at 150 °C must be of the order of 5×10^{-2} M^{-1}s^{-1}).

Next, our study proves that the process $RO_2\cdot + \cdot NO \rightarrow RO\cdot + \cdot NO_2$ takes places at a significant rate under engine-relevant conditions. It produces RO·-dominated radical chain that results in a large number of different products in the presence of NO (primary and secondary alcohols, more aldehydes and acids, and low level of cyclic oxidized products and alkenes), as predicted in Ref. [4]. In contrast to the previous predictions, however, this reaction does not accelerate the autooxidation process noticeably under the conditions of our test. This is likely due to the important radical scavenging reaction $RO_2\cdot + \cdot NO \rightarrow RONO_2$ that decelerates the autooxidation. In result, at least to the order of magnitude, we observe similar oxidation rates in all tests in which NO_x was fed to the autoclave.

Let us finally note that the liquid phase appears to be clear after all tests, and the degradation level is far from producing the characteristic yellow colour of degraded fuel, or phase-separated polar products (sludge).

4. Conclusions

In this work, we designed a test that allows the oxidative degradation of volatile hydrocarbons (components of gasoline) to be studied under conditions that are relevant to the engine cylinder walls and the crankcase, namely high temperature and pressure, and presence of O_2, NO_2 and NO. We demonstrated the capabilities of the bench test by studying the oxidation of isooctane under various conditions. The major findings of the work are:

1. NO_2 initiates an oxidation radical chain process of a significant rate under the studied conditions. Oxygen alone, in the absence of NO_2, cannot produce observable rates of degradation, as predicted in Ref. [4] and proven by test {O_2;*T*}.

2. Nitric oxide, via reaction (2)-(i), tends to produce alkoxy-dominated radical chain (hydrogen abstraction mostly by RO·), as opposed to an alkylperoxy-dominated one (hydrogen abstraction mostly by $RO_2\cdot$). This is proven by the NO-free tests {NO_2;*T*} and {NO_2;*C*}, in which we observed: (i) significantly lower relative concentration of primary and secondary alcohols, which are products of non-selective abstraction of hydrogen from isooctane typical for RO·; (ii) higher concentration of alkenes and tetrahydro-2,2,4,4-tetramethylfuran, which are typical products of $RO_2\cdot$ isomerization. This finding confirms the prediction from our previous work [4].

3. Nitric oxide produces a number of nitrogen-containing compounds that are absent if only NO_2 is fed to the reactor, among them alkyl nitrates and nitroalkanes. This suggests that an important radical scavenging reaction is taking place, $RO_2\cdot + NO \rightarrow RONO_2$, which decelerates the oxidation process. This compensates the acceleration due to the higher reactivity of RO· that dominates the hydrogen abstraction when NO is present. The overall result is that NO changes the composition of the degradation products significantly without changing the oxidation rate drastically.

4. In the absence of nitric oxide, NO_2 produces significant degradation even though no N-containing products are detected. Under the conditions at the cylinder walls, NO_2 does not produce nitrates and nitroalkanes, in contrast with the reports in, e.g., Ref. [24]; NO does.

It should be noted that in the process of formation of gasoline injector nozzle deposits the termination process (11) might be unimportant compared to (2)-(ii): there, the oxidation during the short cycle has been predicted to proceed in accumulation regime [4], where the alkyl peroxy radicals $RO_2\cdot$ are of increasing (instead of steady-state) concentrations and the termination rate is still small. Conversely, in the crankcase the process (11) is most likely essential.

Another interesting finding is that NO produces significant amounts of NO_2 via reaction (4). This process is too slow to change the composition of the quench layer, since the time of the engine cycle is ~50 ms, which is small compared to the characteristic time for oxidation of NO. However, this reaction will decrease the concentration of NO in the crankcase and in the lubricant, compare to Ref. [24].

The procedure and the bench test from our study can be used to investigate a number of other processes and cases important for deposition in gasoline engines, including: (i) study the role of the surface – steel vs. aluminium wall of the cylinder; (ii) other gasoline components (alkenes, arenes); ethanolic gasoline; mixtures of lubricant + gasoline; (iii) various additives of anti-oxidant action (radical scavengers, metal deactivators).

Acknowledgements. The funding and technical support from BP through the BP International Centre for Advanced Materials (BP-ICAM) made this research possible. The work was partly funded by the National Research Foundation (NRF), Prime Minister's Office, Singapore under its Campus for Research Excellence and Technological Enterprise (CREATE) programme. Markus Kraft gratefully acknowledges the support of the Alexander von Humboldt foundation.

References

1. Pearson R, Gold M, Filip S, Turner J, Stetsyuk V, Crua C, et al. Transient effects of fuel sprays on the surface wetting of diesel fuel injectors. Presented at the SAE International Powertrains, Fuels & Lubricants Meeting, Baltimore, Maryland, USA, 24-26 October 2016.
2. Eagle WE, Musculus MPB. Cinema-stereo imaging of fuel dribble after the end of injection in an optical heavy-duty diesel engine. THIESEL 2014 Conf Thermo-Fluid Dyn Process Direct Inject Engines 2014:1–20.
3. Imaoka Y. A study of particulate emission mechanism from injector tip deposit of direct-injection gasoline engines. Presented at the SAE International Powertrains, Fuels & Lubricants Meeting, Gasoline Direct Injection Deposits Workshop, Heidelberg, Germany, 20 September 2018.
4. Slavchov RI, Mosbach S, Kraft M, Pearson R, Filip SV. An adsorption-precipitation model for the formation of injector external deposits in internal combustion engines. Appl Energy 2018; 228:1423–38. https://doi.org/10.1016/j.apenergy.2018.06.130.
5. Aradi AA, Colucci WJ, Scull HM, Openshaw MJ. A study of fuel additives for direct injection gasoline (DIG) injector deposit control. SAE Tech. Paper 2000-01-2020. https://doi.org/10.4271/2000-01-2020.
6. Xu H, Wang C, Ma X, Sarangi AK, Weall A, Krueger-Venus J. Fuel injector deposits in direct-injection spark-ignition engines. Prog Energy Combust Sci 2015; 50:63–80. https://doi.org/10.1016/j.pecs.2015.02.002.
7. Dearn K, Xu J, Ding H, Xu H, Weall A, Kirkby P, et al. An investigation into the characteristics of DISI injector deposits using advanced analytical methods. SAE Int J Fuels Lubr 2014; 7:771–82. https://doi.org/10.4271/2014-01-2722.
8. Ariztegui J. Fast method of generating deposits in GDI engines and analysis of the impact on emissions. Presented at the SAE International Powertrains, Fuels & Lubricants Meeting, Gasoline Direct Injection Deposits Workshop, Heidelberg, Germany, 20 September 2018.

9. Harrison A, Cracknell RF, Krueger-Venus J, Sarkisov L. Branched versus linear alkane adsorption in carbonaceous slit pores. Adsorption 2014; 20:427–37. https://doi.org/10.1007/s10450-013-9589-1.
10. Liu X, Ito S, Wada Y. Oxidation characteristic and products of ETBE (ethyl tert-butyl ether). Energy 2015; 82:184–92. https://doi.org/10.1016/j.energy.2015.01.026.
11. Christensen E, Fioroni GM, Kim S, Fouts L, Gjersing E, Paton RS, et al. Experimental and theoretical study of oxidative stability of alkylated furans used as gasoline blend components. Fuel 2018; 212:576–85. https://doi.org/10.1016/j.fuel.2017.10.066.
12. Marie H, Deeg HP, Philipp H, Marukos N, Wang C. Study of interaction of N-methyl aniline octane booster on lubricating oil. SAE Tech Paper 2018-01–1809. https://doi.org/10.4271/2018-01-1809.
13. Marie H, Rigol S, Deeg HP, Philipp H. Impact of aniline octane booster on lubricating oil. SAE Tech Paper 2016:2016-01–2273. https://doi.org/10.4271/2018-01-1809.
14. Spindt RS, Wolfe CL, Stevens DR. Nitrogen oxides, combustion, and engine deposits. J Air Pollut Control Assoc 1956; 6:127–33. https://doi.org/10.1080/00966665.1956.10467741.
15. Dimitroff E, Moffitt J V, Quillian RD. Why, what and how: engine varnish. Trans ASME 1969; 91:406–16. https://doi.org/10.1115/1.3554951.
16. Hanson JB, Harris SW, West CT. Factors influencing lubricant performance in the sequence VE test. SAE International Fall Fuels & Lubricants Meeting and Exhibition, SAE International 1988; 881581. https://doi.org/https://doi.org/10.4271/881581.
17. Kuhn RR. *ACS Div Petrol Chem Petrol Preprints* 1973; 18:697–8.
18. Johnson MD, Korcek S. Effect of NOx on liquid phase oxidation and inhibition at elevated temperatures. Lubr Sci 1991; 3:95–118. https://doi.org/10.1002/ls.3010030203.
19. Johnson MD, Korcek S, Rokosz MJ. Effects of NOx on inhibition of oxidation by ZDTPS. *Lubr Sci* 1994; 6:247–66. https://doi.org/10.1002/ls.3010060304.
20. Murakami Y, Aihara H. Effect of NOx and unburned gasoline on low temperature sludge formation in engine oil. Int Congr Expo, SAE International 1991; 910747. https://doi.org/https://doi.org/10.4271/910747.
21. Miyata I, Hirano S, Tanada M, Fujimoto K. Mechanism of turbocharger coking in gasoline engines. SAE Tech Paper 2015-01-2029. https://doi.org/10.4271/2015-01-2029.
22. Jao T-C, Passut CA. Application of surfactants in lubricants and fuels. In: Zoller U, ed., Handbook of detergents, part E: applications. CRC Press, Taylor & Francis group, 2009; chapter 13, p. 331–44.
23. Colclough T. Lubricating oil oxidation and stabilisation. In: Scott G, ed., Atmospheric oxidation and antioxidants, vol. 2. Elsevier Science, 1993, chapter 1, p. 1–69. https://doi.org/10.1016/B978-0-444-89616-2.50005-7.
24. Lillywhite JRF, Sant P, Saville SB. Sludge formation: investigation of sludge formation in gasoline engines. Ind Lubr Tribol, 1990; 42:4-10. https://doi.org/10.1108/eb053400.
25. Nakamura K, Matsumoto E, Kurosaka S, Murakami Y. Effect of ventilation and lubricants on sludge formation in passenger car gasoline engines. SAE International Fall Fuels & Lubricants Meeting and Exhibition, SAE International 1988; 881577. https://doi.org/https://doi.org/10.4271/881577.
26. De la Cruz J, Estefan RM. Test apparatus and method for determining deposit formation characteristics of fuels. Patent 5,693,874, United States of America, 2 Dec 1997.
27. Kuprowicz NJ, Ervin JS, Zabarnick S. Modeling the liquid-phase oxidation of hydrocarbons over a range of temperatures and dissolved oxygen concentrations with

pseudo-detailed chemical kinetics. Fuel 2004; 83:1795–801. https://doi.org/10.1016/j.fuel.2004.03.013.
28. Kawamura M, Moritani H, Nakada M, Oohori M. Sludge formation and engine oil dispersancy evaluation with a laboratory scale sludge simulator. SAE International Fall Fuels & Lubricants Meeting and Exhibition, SAE International 1989; 892105. https://doi.org/https://doi.org/10.4271/892105.
29. Moritani H, Shimura Y, Mizutani Y, Hoshino K, Ueda F, Akiyama K. Investigation on oxidation stability of engine oils using laboratory scale simulator. SAE International Fall Fuels & Lubricants Meeting and Exhibition, SAE International 1995; 952528. https://doi.org/https://doi.org/10.4271/952528.
30. Aworinde SM, Wang K, Lapkin AA. Borate-assisted liquid-phase selective oxidation of *n*-pentane. Appl Catal A Gen 2018; 563:28–42. https://doi.org/10.1016/j.apcata.2018.06.023.
31. Slavchov RI, Novev JK, Mosbach S, Kraft M. Vapor pressure and heat of vaporization of molecules that associate in the gas phase. Ind Eng Chem Res 2018; 57:5722–31. https://doi.org/10.1021/acs.iecr.7b04241.
32. Pádua AAH, Fareleira JMNA, Calado JCG, Wakeham WA. Density and viscosity measurements of 2,2,4-trimethylpentane (isooctane) from 198 K to 348 K and up to 100 MPa. J Chem Eng Data 1996; 41:1488–94. https://doi.org/10.1021/je950191z.
33. Amara BA, Nicolle A, Alves-Fortunato M, Jeuland N. Toward predictive modelling of petroleum and biobased fuel stability: kinetics of methyl oleate/n-dodecane autooxidation. Energy and Fuels 2013; 27:6125–33. https://doi.org/10.1021/ef401360k.
34. Denisov ET, Afanas'ev IB. Oxidation and antioxidants in organic chemistry and biology, 1st ed. CRC Press, Taylor & Francis group, 2005.
35. Zabetakis MG, Scott GS, Jones GW. Limits of flammability of paraffin hydrocarbons in air. Ind Eng Chem 1951; 43:2120–4. https://doi.org/10.1021/ie50501a041.
36. Zabetakis MG. Flammability characteristics of combustible gases and vapors. Washington, US Dept of the interior, Bureau of Mines, 1965, bulletin 627.
37. Coward HF, Jones GW. Limits of flammability of gases and vapors. Washington, US Dept of the interior, Bureau of Mines, 1952, bulletin 503.
38. Bamford CH, Tipper CFH (editors). Comprehensive chemical kinetics: liquid-phase oxidation. Elsevier: Amsterdam, Netherlands, 1980.
39. Flasińska P, Fraczak M, Piotrowski T. Explosion hazard evaluation and determination of the explosion parameters for selected hydrocarbons C6-C8. Cent Eur J Energ Mater 2012; 9:399–410.
40. Setchkin NP. Self-ignition temperatures of combustible liquids. J Res Natl Bur Stand (1934) 1954; 53:49. https://doi.org/10.6028/jres.053.007.
41. Huie RE. The reaction kinetics of NO_2. Toxicology 1994; 89:193–216. https://doi.org/10.1016/0300-483X(94)90098-1.
42. Tsukahara H, Ishida T, Mayumi M. Gas-phase oxidation of nitric oxide: chemical kinetics and rate constant. Nitric Oxide - Biol Chem 1999; 3:191–8. https://doi.org/10.1006/niox.1999.0232.
43. Levenspiel O. Chemical reactor engineering, 3rd ed. John Wiley & Sons; 1999.
44. Fish A. Radical rearrangement in gas-phase oxidation and related processes. Q Rev Chem Soc 1964; 18:243–69. https://doi.org/10.1039/qr9641800243.
45. Chen C-I, Hsu SM. A chemical kinetics model to predict lubricant performance in a diesel engine. Part I: simulation methodology. Tribol Lett 2003; 14:83–90. https://doi.org/10.1023/A:1021748002697.

46. Diaby M, Sablier M, Le Negrate A, El Fassi M, Bocquet J. Understanding carbonaceous deposit formation resulting from engine oil degradation. Carbon 2009; 47:355–66. https://doi.org/10.1016/j.carbon.2008.10.014.
47. E. T. Denisov, I. V. Khudyakov. Mechanism of action and reactivities of the free radicals of inhibitors. Chem. Rev. 1987; 87:1313-57. https://doi.org/10.1021/cr00082a003.
48. E. Ya. Davydov, S. Korcek, R. K. Jensen, G. E. Zaikov. Kinetics and mechanism of liquid-phase nitration of 2,4,5-tri-t-butylphenol. Intern. J. Polymeric Mater. 1997; 37:201-16. https://doi.org/10.1080/00914039708031485.